

Active control of turbulent boundary layers

By RUBEN RATHNASINGHAM†
AND KENNETH S. BREUER

Brown University, Division of Engineering, Providence, RI 02912, USA

(Received 1 April 2002 and in revised form 30 June 2003)

An experimental investigation is made into the active control of the near-wall region of a turbulent boundary layer ($Re_\theta = 1960$) using a linear active control scheme. System identification in the boundary layer provides optimal transfer functions that predict the downstream characteristics of the streamwise velocity fluctuations. Enhanced detection techniques isolate the large-scale turbulent motion and improve the downstream correlations, resulting in greater controllability. The control is applied using a spanwise array of resonant synthetic jet actuators that introduce pairs of streamwise vortices into the flow. Control results show that a maximum reduction of 30% in the streamwise velocity fluctuations is achieved. This reduction is greatest at the point of optimization but spans a few hundred viscous lengths downstream of the actuator, about 50 viscous lengths in the wall-normal direction and 150 viscous lengths in the spanwise direction. The wall pressure fluctuation and the mean wall shear stress (measured approximately using mean velocity profiles near the wall) were reduced by 15% and 7% respectively. The bursting frequency, based on VITA event detection was also reduced by up to 23%.

1. Introduction

Advances over the past twenty years in the understanding of near-wall turbulent shear flow structure have resulted in several suggestions for active control of turbulence with an aim of reducing turbulent fluctuations and minimizing turbulent skin friction. With the development of large-scale numerical simulations, a wide variety of control mechanisms have been explored numerically. These include control schemes based on qualitative physical arguments (Choi, Moin & Kim 1994; Schoppa & Hussain 1998), formal optimal and sub-optimal control theory (Bewley, Moin & Temam 2001), neural networks (Lee *et al.* 1997) and reduced-order dynamical representations of the near-wall region of the turbulent shear flow (Coller, Holmes & Lumley 1994). The numerical investigations have focused on turbulent drag reduction, and indicate that reductions of the order of 15–20% can be achieved, although the simulations are all at very low Reynolds numbers and usually assume a dense and uniform network of both sensors and actuators on the wall.

For a variety of reasons, practical demonstrations of turbulence control have been more difficult to achieve. The small length and time scales that characterize turbulent flows make the design and fabrication of arrays of sensors and actuators very challenging. Although microelectromechanical systems (MEMS) can, in principle,

† Present Address: Neural Engineering Laboratory, University of Michigan, 300 N. Ingalls Bldg., #900F Ann Arbor, MI 48109, USA.

meet these requirements, they have not yet been successfully used for fully integrated turbulence control, but only as demonstrations of what might be achieved (Tsao *et al.* 1997). Nevertheless, some experimental demonstrations of the effects of actuation on turbulent flows have been presented. Both Wilkinson & Balasubramanian (1985) and Gad-el-Hak & Blackwelder (1989) showed that selective actuation in a fully turbulent flow could affect the streaky structure in the flow and were suggestive of what might be achieved with a more systematic control design. These studies were also limited by the available hardware, and did not attempt to implement more than a single sensor/actuator pair. More importantly, they did not attempt to apply any formal control theory to the problem, but relied on a more intuitive approach which, while valid as a first step, will never ultimately be an approach to successful control. More recently, Jacobson & Reynolds (1998) did employ a formal control system to inhibit the development of streamwise streaks in a laminar water channel flow, seeded with synthetic streamwise vortices. This demonstration was valuable because it demonstrated the successful use of sensors and actuators coupled to an appropriate control algorithm, albeit in a surrogate for the fully turbulent boundary layer.

The first demonstration of real-time active control in a fully turbulent flow was presented in a short note by Rathnasingham & Breuer (1997*b*) who used an array of three wall-based shear sensors coupled to a single wall-based synthetic jet actuator. A feedforward control algorithm, based on the short-term linear dynamics of the near-wall turbulent boundary layer, was used to minimize turbulent fluctuations at a single control point downstream of the actuator. Their results demonstrated a 31% reduction in u_{rms} (measured at $y^+ = 12$) and a 17% reduction in the wall pressure fluctuations.

The results in the present paper form a more complete report of the progress that has been achieved since the first results of Rathnasingham & Breuer (1997*b*). The details of the control architecture and its performance are presented in full, and experimental results from a more extensive control matrix (three actuators) are presented. The structure of the paper is as follows. The following section describes the control strategy which consists of two parts: a flow prediction leg, which relates sensor signals to flow structures at the downstream control points, and an active control leg, which uses that information to achieve a given control objective by minimizing a cost function. Section 3 describes the experimental results obtained, including the performance of the forward prediction and active control legs, as well as details on the effect of the control on the small-scale structure of the turbulent boundary layer. Section 4 completes the paper with concluding remarks and recommendations for future work.

2. Linear control strategy

The control approach is based on two key assumptions: (i) the majority of the turbulence-producing events in the near-wall region of the flow are associated with the large-scale ‘coherent structures’ and (ii) these coherent structures may be modelled (for short times) by dynamical equations which are linear with respect to the mean flow. The first assertion is supported by a large body of research on coherent structures over the past twenty years, and is well-illustrated in the analysis performed by Johansson, Alfredsson & Kim (1991) of numerically generated turbulence in which they report that the coherent structures, while only occupying 25% of the volume in the near-wall region, are responsible for 50% of the total turbulence production. The assumption of linearity is based on the observation that the strong mean shear of the near-wall

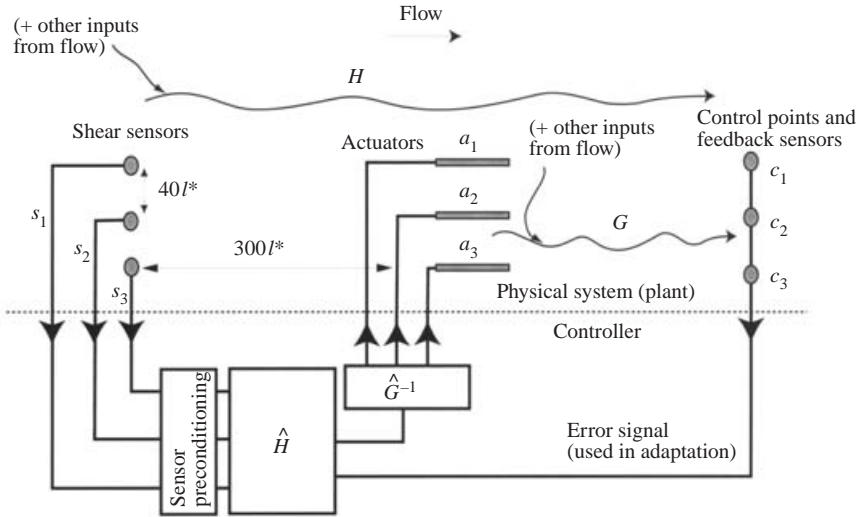


FIGURE 1. Schematic diagram showing the plant – the turbulent boundary layer – together with detection sensors (s_1, s_2, s_3), actuators (a_1, a_2, a_3) and downstream control points (c_1, c_2 and c_3). The block diagram below the dotted line represents the controller including the adaptive feedback path (which was not used in the current experiments). H and G are actual transfer functions, while \hat{H} and \hat{G} are their linear estimates, derived from cross-correlation measurements.

turbulent flow will dominate the short-time evolution of small perturbations. This is consistent with the framework provided by the rapid distortion theory of turbulence (Hunt & Carruthers 1990) and other models for near-wall turbulence (Landahl 1990). In addition, experiments by Johansson, Her & Haritonidis (1987) found that conditionally sampled u , v and p signals scaled linearly with threshold amplitude, again suggesting an amplitude-invariant behaviour for these coherent structures. For the purposes of control, this linearity assumption need only hold for the short time it takes a structure to advect from an upstream sensor to an actuator, and does not imply that turbulence production as a whole is governed by a linear mechanism.

Given these working assumptions, the control strategy pursued in these experiments is shown schematically in figure 1. A multiple-input, multiple output (MIMO) linear filter (Bendat & Piersol 1971) is constructed as an estimate of the transfer function between signals from a spanwise array of N upstream wall-based sensors (in this case $N = 3$: $s_1(t)$, $s_2(t)$ and $s_3(t)$) and the signals from sensors located at M downstream ‘control points’ (again, in this case, $M = 3$: $c_1(t)$, $c_2(t)$ and $c_3(t)$). The estimated transfer function is represented in figure 1 as \hat{H} , while the physical (true) relationship between the upstream and downstream sensors is indicated by H . In general H will not be equal to \hat{H} , the difference resulting from both a nonlinear relationship between the two arrays of sensor signals and the fact that the signals at the downstream sensor array will also be affected by other inputs not sensed by the upstream sensor array (for example, outer-flow structures, etc.).

In a similar manner, we construct a linear transfer function between the input signal to an array of P actuators (in this case $P = 3$) and the measured output signal at each of the downstream control points. This transfer function, \hat{G} , represents the linear combination of actuator dynamics, the interaction between the actuator output flow and the near-wall turbulent structures, and their advection downstream to the control

points. As before, the ‘true’ relationship between the signal input to the actuators and the signal measured at the control points is nonlinear and includes additional inputs, not captured by this simplified representation.

With these two transfer functions (or, more correctly, systems of transfer functions), we invert the actuator transfer function and construct a feedforward control system, $\hat{H}\hat{G}^{-1}$, such that if \hat{H} and \hat{G} were completely accurate descriptions of the full system, the fluctuating signal at each control point, c_k , would be zero. In reality, modelling errors, noise and more importantly nonlinearities and non-observed inputs will result in an error at the control points such that the difference between the predicted signal at the control points and the observed signal will not be identically zero. However, this error can be further minimized, and maintained at a low level by employing an adaptation scheme. Typical adaptation schemes (Nelson & Elliot 1992) include perturbing the filter coefficients, either randomly or by some proscribed adaptive optimization scheme. In this manner, the overall control performance can be optimized or adapted to adjust to changing free-stream conditions. Adaptation was not attempted in the experiments reported here.

This control system is closely modelled on the feedforward control systems used with considerable success in the active control of sound (Nelson & Elliot 1992). However, it is important to be clear that a feedforward approach can only be applied if the action of the actuators does not affect the signal measured at the upstream sensors. In some situations there may be an important modification of the upstream signal by the actuators (coupled, for example, with upstream-propagating acoustic waves), in which case a more complex *feedback* system must be adopted. The term ‘feedforward control’ is interpreted in different ways by different segments of the control community. The present approach is firmly within Nelson & Elliot’s definition of feedforward, but in order to avoid possible confusion with other research, we avoid that terminology for the moment and simply refer to the present scheme as ‘active control’.

As presented here, the control approach is quite general and may be applied to an arbitrary number of upstream sensors, actuators and downstream sensors (control points). It has several appealing features:

(a) Different choices for the sensor at each control point, and the signal used from those sensors enables a wide range of control objectives. For example, choosing the control point to be a velocity sensor in the near-wall region, and its associated signal to be the r.m.s. velocity, leads to a control system that minimizes turbulent fluctuations at the control points. Choosing the control signal to be r.m.s. pressure fluctuations from an array of wall pressure sensors leads to the minimization of turbulent pressure fluctuations. Selecting the signal to be a moving average of the signal from a wall shear sensor will yield a control scheme optimized to reduce the mean drag. Each of these control objectives is different and will not necessarily result in the same filters, \hat{H} and \hat{G} . However, they all can be treated using this approach.

(b) In the most general sense, the control filters depend on inputs measured in space and time. For example, one possible series of filters could be constructed from a large spatial template of wall sensors, all sampled at a single time. A second extreme might be a strictly temporal filter, constructed from a single sensor, sampled over time and used to construct the estimate at the control point. The optimal filter is one that contains both spatial and temporal information.

(c) Since the spatial correlation of the turbulent flow is finite, we can assume that the spatial template of sensors required to control a specific area is also finite. Larger areas of controlled flow might then be achieved by coordinating a ‘quilt’ of local

controllers, each controlling a small patch of flow. The way in which this would be accomplished is not trivial, but does imply that the scaling up of this control approach to cover larger areas should not be an unreasonably difficult task.

2.1. Sensor pre-conditioning: detection of large-scale structures

Central to the success of this scheme is the ability to accurately predict the flow state at the downstream sensors, c_k , using the upstream wall sensors, s_i . For the turbulent boundary layer, the dominant contribution over such large distances is by the large-scale structures. However the 'footprint' of these structures is contaminated by random variations and small-scale fluctuations. Thus the chief problem of prediction becomes one of identification of the large-scale structures and prediction of their evolution. If we assume that we can define large-scale structures statistically, i.e. any signal that retains finite correlation over some spanwise distance, then the identification can be efficiently achieved using a *conditioned spectral analysis* (Bendat & Piersol 1971) which isolates the correlated portion of (any) two signals. This is best expressed in the frequency domain:

$$\begin{aligned} S_{12}^c(\omega) &= \frac{\Phi_{12}(\omega)}{\Phi_{22}(\omega)} S_1(\omega) \\ &= L_{12}(\omega) S_1(\omega). \end{aligned} \quad (2.1)$$

S_{12}^c is the correlated part of the two signals S_1 and S_2 ($s_1(t)$ and $s_2(t)$ expressed in the frequency domain), Φ_{12} and Φ_{22} are the cross-spectra and auto-spectra respectively. Note that for a spatially homogeneous field (such as the spanwise direction in a turbulent boundary layer), S_{12}^c is identical to S_{21}^c . The rest of the signal makes up the uncorrelated portion, S_{12}^u :

$$S_{12}^u(\omega) = S_1(\omega) - L_{12}(\omega) S_1(\omega). \quad (2.2)$$

The conditioning filter, L_{12} , is nothing more than a linear filter which pre-conditions the input signals, weighting them to favour a frequency band statistically determined to be most highly correlated. In this sense, it is a rather crude pre-conditioning and many more complex pre-conditioning schemes can be envisaged, particularly if a dynamic model of the near-wall region of the boundary layer were available. In this case a Kalman filter (Brown & Hwang 1997) could be constructed, as was demonstrated in a low-order numerical simulation by Podvin & Lumley (1998). This would give a real-time identification of large-scale structures and, presumably, a superior performance over the simple case presented here.

2.2. Forward prediction and the Wiener filter

With the pre-conditioned input signals, we now need to assemble the filter that will predict the evolution of the large-scale structures (\hat{H} in figure 1). We consider a system with N input signals ($s_1, s_2, \dots, s_i, \dots, s_N$) and M control points ($c_1, c_2, \dots, c_k, \dots, c_M$). The predicted signal at the k th control point at any given time, t_o , is described by a weighted sum:

$$\widehat{c_k(t_o)} = h_{1k} \cdot s_1 + h_{2k} \cdot s_2 + \dots + h_{ik} \cdot s_i + \dots + h_{Nk} \cdot s_N \quad (2.3)$$

where h_{ik} are linear weights (assumed to be constant). Note that the s_i are discrete measurements from any combination of spatially or temporally distinct sensors. For example s_1 could be a measurement from an upstream shear sensor, sampled at $t = t_o$; s_2 might be a measurement from the same sensor, but sampled at a previous

time, $t = t_o - \Delta t$; s_3 might be a measurement from a different sensor, sampled at $t = t - 2\Delta t$, and so on. (The implications of this will be discussed in the next section.)

The values of h_{ik} are found by minimizing the mean-square error between the real measurement at the control point $c_k(t)$, and the predicted measurement at the control point, $\widehat{c_k(t)}$. This least-squares minimization procedure is simply one definition of the Weiner filter (Bendat & Piersol 1971), and after some rudimentary calculations, we find that the linear weights, h_{ik} , are the solution to the matrix equation:

$$\begin{bmatrix} \Phi_{11} & \Phi_{12} & \dots & \Phi_{1N} \\ \Phi_{21} & \ddots & & \\ \vdots & & \ddots & \\ \Phi_{N1} & & & \Phi_{NN} \end{bmatrix} \begin{bmatrix} h_{1k} \\ h_{2k} \\ \vdots \\ h_{Nk} \end{bmatrix} = \begin{bmatrix} \Psi_{1k} \\ \Psi_{2k} \\ \vdots \\ \Psi_{Nk} \end{bmatrix} \quad (2.4)$$

where Φ_{ij} is the mean cross-correlation between different input signals:

$$\Phi_{ij} = \langle s_i s_j \rangle \quad (2.5)$$

and Ψ_{ik} is the cross-correlation between each input signal and the k th control point.

$$\Psi_{ik} = \langle s_i c_k \rangle. \quad (2.6)$$

These cross-correlations can be computed from measurements and the matrix inverted to yield the weights. The process can be repeated with different right-hand sides ($k = 1 \dots M$) to find weights connecting the input sensor array to each of the control points.

2.3. Filter design flexibility

As mentioned above, the input measurements can be taken from any point in space or time. This flexibility has many interesting implications, a few of which are discussed here. If all the inputs are taken from spatially distinct sensors at a single time, $t = t_o$, and used to predict the flow at the control point at the same time, t_o , then the Weiner filter will contain no flow history, but will rely solely on the spatial pattern of the flow to predict its state at some other point. This was explored by Almonlirdvirman & Breuer (2000) using the flow from a low-Reynolds-number turbulence database. It is also identical (mathematically) to stochastic estimation (Adrian 1994). At the other extreme, if we use a single sensor, but sample it at many times and use that time history to predict the flow at some later time, then we are relying solely on the temporal evolution of the flow at a single point to predict the state of the flow at some other point. The linear filter (2.3) then reduces to

$$c(t_o) = h_o \cdot s(t_o) + h_1 \cdot s(t_o - \Delta t) + \dots + h_i \cdot s(t_o - i\Delta t) + \dots + h_N \cdot s(t_o - N\Delta t) \quad (2.7)$$

from which it is easy to see that the elements of the matrix in the Weiner filter equation (2.4) reduce to the standard auto- and cross-correlation functions, $R_{ss}(\tau)$ and $R_{sc}(\tau)$. Clearly both of these extremes are limited in their ability to accurately predict the flow at some remote point in space and some future time, and the optimal filter must contain some spatial information (derived from distinct input sensors) as well as some temporal history (derived from a time sequence sampled at each sensor).

Another interesting implication of this approach stems from the fact that the forward prediction equation (2.3) can use sensor inputs that come from times in the future ($t > t_o$). It is, of course, not physically possible to implement this kind of filter directly. However, such infinite impulse response (IIR) filters can be re-cast as recursive filters that can be physically implemented. This is commonly done in control

systems design, but can be subtle, and is beyond the scope of the current discussion. For the experiments described here, only finite impulse response (FIR) filters, which rely only on measurements from past times ($t \leq t_o$) were used.

Using the methods described above, \hat{H} can be constructed connecting N sensor inputs drawn from time and space to each of the M control points. In the most general form this leads to M filters, each with N weights. Similarly, the relationship between each of the P actuators and the output signals at each of M control points can also be identified by simply measuring the transfer function (i.e. cross-correlation) between a signal injected into the actuator and the correlated response at each of the control points. This results in $P \times M$ filters representing \hat{G} in figure 1. By inverting the entire system, a single system of filters, $\hat{H}\hat{G}^{-1}$, is constructed such that the sensor inputs drive the actuator array so that, in the absence of nonlinearity, unobserved inputs, noise and estimation errors, the signal measured at the control points will be identically zero. It is this system that is implemented and evaluated in the following discussion.

Without question, this form of forward prediction represents a crude first attempt, and one which could be improved dramatically by the incorporation of some understanding of the near-wall dynamics of the turbulent flow. The use of a model-based estimator, such as a Kalman Filter (Brown & Hwang 1997) based on either the full Navier–Stokes equation, a linearized version (the Orr–Sommerfeld and Squire equations) or a reduced-order system (Waleffe 1997; Podvin & Lumley 1998) would probably yield a more accurate estimation of the flow state, and improve the subsequent control performance. However, for the present investigation, the simple Weiner filter was sufficient to establish the principle of the control system operation, and these improvements are left for future experiments.

3. Experimental results and discussion

Having laid the groundwork for the control scheme, we present a demonstration of its performance. In the current experiment a limited extent of turbulent boundary layer is controlled using three input sensors, three actuators and three control points. The details and results are discussed in this section.

3.1. Experimental setup

All experiments were carried out in a low-turbulence wind tunnel previously described in some detail by Breuer *et al.* (1996). An aluminium flat plate (0.6 m wide, 2.5 m long) was mounted vertically in the wind tunnel test section which measures $0.3 \times 0.6 \text{ m}^2$ in cross-section, and 3 m in length. A roughness strip 10 cm downstream of the leading edge tripped the boundary layer which was then allowed to grow undisturbed. Careful measurements ensured the existence of a canonical zero-pressure-gradient turbulent boundary layer. At the operating speed of 6 m s^{-1} , the Reynolds numbers based on downstream distance from the leading edge and momentum thickness are 8.1×10^5 and 1960, respectively. The corresponding viscous length and time scales are $u_\tau = 0.31 \text{ m s}^{-1}$, $l^* = 55 \mu\text{m}$ and $t^* = 270 \mu\text{s}$. To ensure the statistical convergence of the measured data, record lengths are based on a 95% confidence level with a 0.2% uncertainty in the root-mean-squared value. This resulted in data records that contained 2×10^6 independent sample points each. The active control system was managed with a 60 MHz DSP-based real-time signal-processing board embedded in a desktop PC. The board was capable of running the control system (three inputs and three outputs in the cases presented here) at a maximum of 35 kHz ($9.5 f^*$) – much

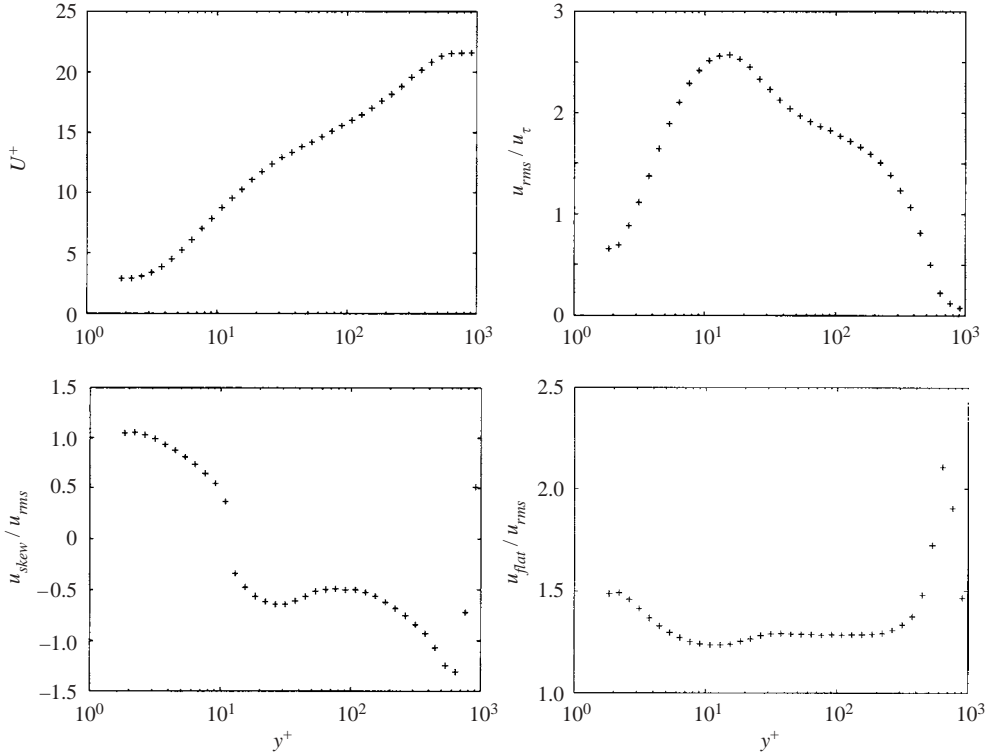


FIGURE 2. Wall-normal profiles of the first four statistical moments of the streamwise velocity in the turbulent boundary layer ($Re_\theta = 1960$).

faster than was actually required. Further details of the implementation of the control loop are discussed by Rathnasingham (1997).

The baseline turbulent boundary layer velocity profiles are shown in figure 2. These profiles, and all subsequent boundary layer measurements were obtained using a single-wire hot wire probe, $2.5\ \mu\text{m}$ in diameter, operated at a resistive overheat ratio of 1.6. The probe was mounted on a traversable sting controlled by the lab computer. The profiles compare well with past low- Re data (Purtell, Klebanoff & Buckley 1981). The mean velocity profile is seen to exhibit a linear near-wall region for $y^+ < 7$, a log-law region for $30 < y^+ < 100$ and a outer wake region for $y > 200$. The logarithmic region is well-matched to the Clauser profile with a gradient of 2.5 and an intercept of 5.0 (Schlichting 1968). The mean wall shear stress, obtained using the Clauser profiles, was $0.116\ \text{N m}^{-2}$, corresponding to a friction velocity, $u_\tau = 0.31\ \text{m s}^{-1}$. The peak value in the root-mean-squared profile ($u_{rms} = 2.6u_\tau$) occurs at $y^+ = 12$ and coincides with the zero-crossing of the skewness and the point of minimum flatness.

3.2. Sensing and forward prediction

3.2.1. Input sensors

Shear stress sensors were chosen as the primary input sensors for the control scheme. These meet the requirement that they are non-invasive to the boundary layer, and are a more accurate estimation of the local boundary layer structure than surface pressure measurements (Kravchenko, Choi & Moin 1993). For these experiments, the shear stress sensors used were flush-mounted hot wires, operated in a constant-temperature

mode. Rathnasingham & Breuer (1997b) reported that the shear sensors were more effective when they were oriented so that the hot wire was parallel to the mean flow, rather than perpendicular, as is the usual orientation. In this parallel mode, the wires are primarily sensitive to the absolute value of the spanwise shear fluctuations, but also retain some sensitivity to streamwise shear fluctuations. The improvement in control performance due to this unconventional use of the shear sensors is still an issue that needs to be explored, but it is consistent with observations in a numerical approach to turbulence control by Lee *et al.* (1997), who found that the spanwise shear is an effective control input for turbulent shear flows. The alignment of the wire also gives the sensor extremely good spatial resolution in the spanwise direction (limited by the thickness of the sensing wire which for these experiments was $2.5\ \mu\text{m}$ – less than $l^*/20$). The streamwise resolution of the sensor (dictated by the length of the sensing wire) is somewhat worse (in our case about $10l^*$). However, this preferential sensitivity matches the shape of the flow structures we are trying to detect which are typically greatly elongated in the streamwise direction. This geometric factor might be one reason for the observed improvement in control performance.

Pressure sensors were used for the experiments to control the wall pressure fluctuations. The measurements were taken using Knowles BL-1785 microphones calibrated with an accurate 1/4 in. Bruel & Kjaer microphone whose frequency response was uniform from 30 Hz to 12 kHz. The microphones were mounted in the flat plate with an access hole measuring 1 mm in diameter or $20l^*$, which was found (Schewe 1983) to be the maximum allowable transducer size for the accurate measurements of the most significant contributions to the wall pressure signal. Acoustic fluctuations due to the ambient noise in the wind tunnel environment can mask the turbulent pressure fluctuations. This mode of interference was minimized by using a variant of the conditioned spectral response technique described earlier. In this case, however, the objective was to subtract from the signal the component due to pressure fluctuations that are correlated over long distances (much longer than flow structure pressure fluctuations). Thus, a far-field pressure sensor was placed several centimetres from the control region. The correlated portion of the two signals (which is due to acoustic modes) was determined using the conditioned spectral response technique and subtracted from the microphone signals prior to any control system processing. (This technique was also successfully employed by Naguib, Gravante & Wark 1996.)

3.2.2. Conditioned spectral response and the performance of the forward prediction

As described in §2.1, the conditioned spectral response (CSA) was used to emphasize large-scale (coherent) structures common to two adjacent sensors. Figure 3 shows the structure of the CSA filter, L_{12} , that was derived from two adjacent spanwise wall-shear sensors, separated by $40l^*$ in the spanwise direction. As one might expect, it has the form of a low-pass filter, emphasizing the low frequencies that are associated with the elongated low-speed streaks. It should be noted that a property of the symmetric FIR filter that results from the CSA procedure is that the resultant feature has linear phase, the slope of which represents the average advection time between the two sensors. In this case, since the two sensors are side-by-side with no streamwise offset, the phase is identically zero.

Several combinations of raw input signals and their respective conditioned signals were used to compute the forward predictor, \hat{H} . Figures 4 and 5 show the r.m.s. error between the predicted and measured velocity fluctuations for several different sensor configurations. It is clear that the sensors that are relatively close together ($40l^*$) perform better in predicting the downstream flow patterns than the configurations

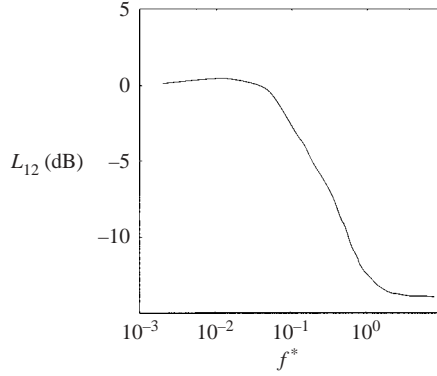


FIGURE 3. The filter L_{12} illustrating the emphasis on the low-frequency scales. The filter was used to condition the signals from the detection sensors so as to extract the large-scale motion in the flow.

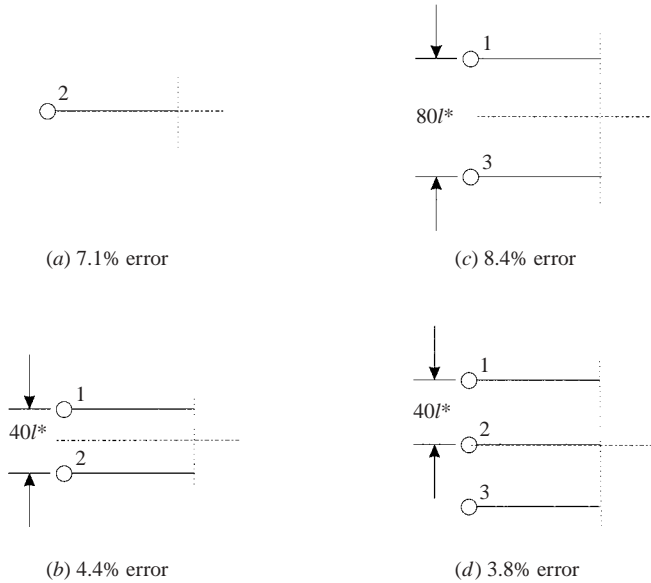


FIGURE 4. Schematic layout of different configurations of raw sensor inputs without pre-conditioning, and their respective performance, measured in terms of the r.m.s. error between the predicted velocity fluctuations and the measured velocity fluctuations $300l^*$ downstream of the sensor line.

that have more widely spaced input sensors. This is not surprising since it is well-known that the spanwise extent of the low-speed streaks is approximately $50l^*$, and so the closer-spaced sensor pair is more capable of picking this out reliably. It is also clear from figure 5 is that the CSA does very well in improving the predictive performance. Indeed, the benefit of the CSA is as great as the benefit of adding additional sensors. What is also remarkable is the fact that the error $300l^*$ downstream is as small as 3%, given the rather limited nature of the input signals. This results lends credence to the belief that the short-term dynamics of the large-scale structures in the near-wall region of the turbulent boundary layer may be described by a linear dynamical system which is adequate for the purposes of active control.

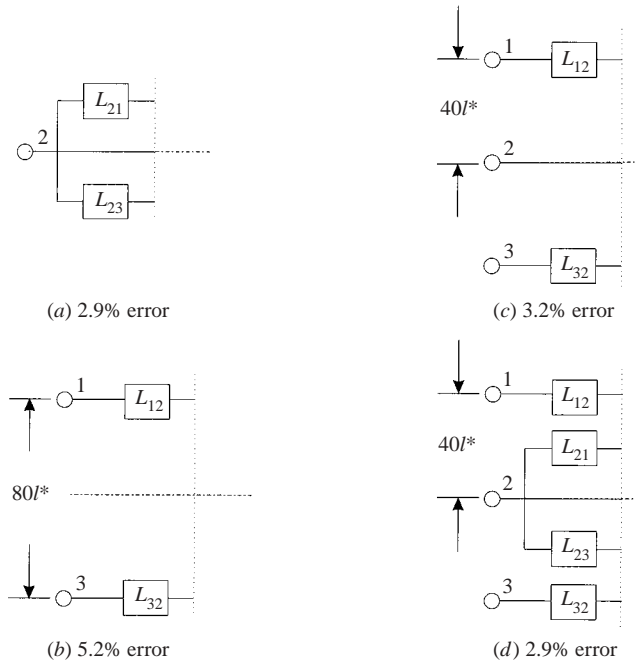


FIGURE 5. Schematic layout of different configurations of sensor inputs, utilizing pre-conditioning, and their respective performance, measured in terms of the r.m.s. error between the predicted velocity fluctuations and the measured velocity fluctuations $300l^*$ downstream of the sensor line.

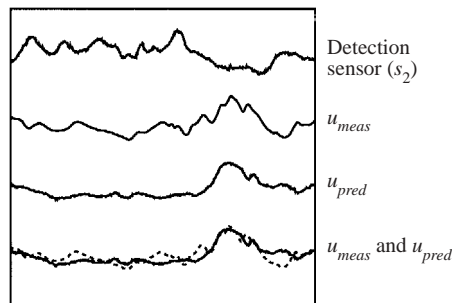


FIGURE 6. Sample time series, showing the signal from the middle shear sensor s_2 , as well as the measured and predicted streamwise velocity ($300l^*$ downstream) and the two superimposed for comparison. The signals were recorded with the actuator disconnected.

The configuration illustrated in figure 5(d) yielded the optimum predictive performance, with an r.m.s. error of less than 3%. This configuration was used for subsequent experiments. A sample time-trace of the centreline input signal, s_2 , the predicted velocity fluctuation $300l^*$ downstream and the measured velocity fluctuations is shown in figure 6. Comparing the measured and predicted velocity signals, it is clear that the large-scale motion, high-amplitude peaks and periods of activity and lull are successfully captured. The small-scale features of the signal, representing the small-scale sub-inertial eddies, are not captured well, although these are assumed to be of little dynamical significance in the overall turbulence production cycle.

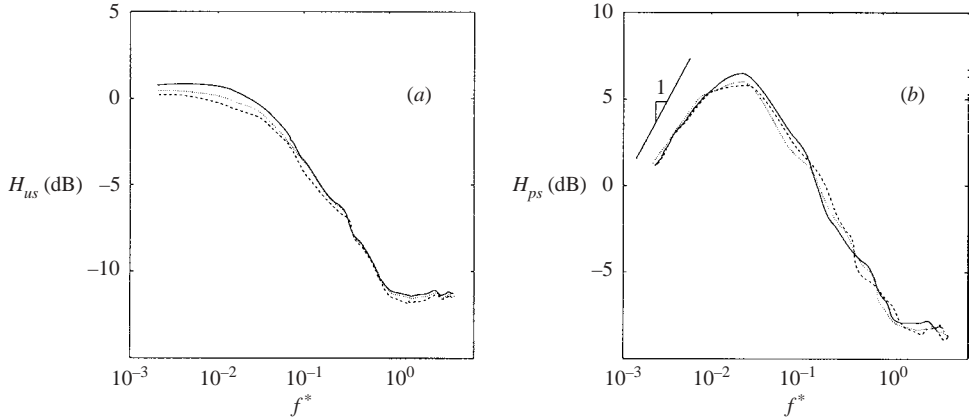


FIGURE 7. Optimal multiple-input/single-output transfer functions for each of the three detection sensors. (a) Prediction of streamwise velocity $300l^*$ downstream of the sensor plane and at $y^+ = 10$. (b) Prediction of the wall pressure $500l^*$ downstream of the sensor plane.

The phase response (not shown here) exhibits a constant slope (always true for a symmetric FIR filter), which corresponds to an average convection speed between the sensor and the control point of $u_c^+ = 10.7$. This closely matches the typical convection speed of the large-scale structures of 10.3 found by Johansson *et al.* (1991). This lag was seen to be constant for all cross-spectra between the upstream and downstream sensors.

The optimal sensor configuration (figure 5d) for the prediction of the streamwise velocity fluctuation was also used for the prediction of the wall pressure fluctuation, this time located $500l^*$ downstream of the detection sensors. The characteristics of the resultant filters are illustrated in figure 7. The optimal transfer functions for the streamwise velocity ($300l^*$ downstream of the sensor plane) are shown in figure 7(a). As one might expect, the emphasis is on the low frequencies ranging up to the inertial scales and the character of the transfer function is simply a low-pass filter. The filters for the wall pressure ($500l^*$ downstream of the sensor plane) are shown in figure 7(b) and tend to emphasize higher frequencies. Note that the low-frequency slope is approximately equal to 1, which corresponds to a first derivative in the time domain ($\partial/\partial t = i\omega$, where $i = \sqrt{-1}$). Using a Taylor hypothesis to equate time derivatives with streamwise gradients, this filter structure indicates that the wall pressure is a function of the gradient of the upstream wall shear – an observation consistent with previous conditional sampling of velocity and pressure, for example, by Johansson *et al.* (1991), who show that the high-amplitude pressure peaks coincide with large positive gradients in the streamwise velocity fluctuations.

3.3. Actuation and fixed-amplitude forcing

The second half of the control setup is the actuation of the flow. The flush-mounted actuator used in these experiments is a zero-net-mass-flux jet (or ‘synthetic jet’) similar to those introduced initially by Ingard (1953), but applied to problems in flow control in recent years primarily by Glezer and co-workers (Glezer & Amitay 2002). The present devices, schematically illustrated in figure 8, are modified from Glezer’s design to enable close packing in the spanwise direction and to generate a disturbance suitable for boundary layer control. The exit slit, measuring $10l^*$ by $150l^*$, is flush with the surface and aligned in the streamwise direction. Hot-wire

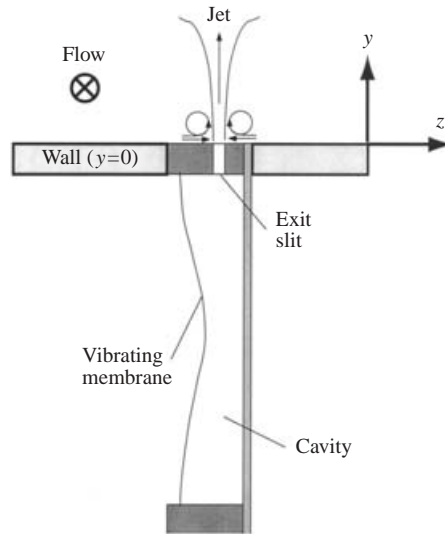


FIGURE 8. Schematic diagram of the actuator, shown in the cross-stream plane, with the resultant jet flow out of the exit slit. The boundary layer flow is out of the page, and actuators are stacked side-by-side in the spanwise direction with a centre-to-centre separation of $40l^*$.

measurements (Rathnasingham & Breuer 1997a), as well as related computational simulations (Lee & Goldstein 2002) and PIV measurements (Wu & Breuer 2003) indicate that the flow generated by the actuator is a series of streamwise-oriented vortex pairs generated with each outstroke of the membrane which quickly merge to form a jet. The device is operated at the structural resonance of the membrane and by tailoring the membrane and cavity dimensions this resonant frequency and the jet properties can be tailored (Rathnasingham & Breuer 1997a). In the present case, the carrier frequency was 2.3 kHz which corresponds to $f^* \approx 0.62$ – well into the dissipation range and above the frequencies of any energy-containing eddies in the boundary layer. This high-frequency operation means that the external flow quickly damps out the unsteady vortex production associated with each membrane cycle, and the time-integrated effect is a quasi-steady jet directed upwards and located at the actuator exit accompanied by a return flow pulling fluid down and in from each side. This pattern is similar to that used by Jacobson & Reynolds (1998) in their study of control of vortices in laminar boundary layers. The average velocity generated by the control jet could be varied from zero to 1.5 m s^{-1} ($4.8u_\tau$), controlled by amplitude modulation of the carrier wave.

To quantify the effect of the steady unmodulated synthetic jet on the near-wall region of the fully turbulent flow, the streamwise velocity was measured in a (y, z) -plane, downstream of the actuator slit while operating the actuator at a constant amplitude ($1u_\tau$). Figure 9 illustrates the flow pattern as a contour map (in the y, z -plane). The actuator generates a region of low-speed fluid immediately above the actuator exit area due to the pumping of low-streamwise-momentum fluid upwards. This artificially created velocity defect was mapped out in some detail by Lorkowski, Rathnasingham & Breuer (1997) and has the gross characteristics of a naturally occurring low-speed streak: it is centred at about $y^+ = 20$ and is approximately $40l^*$ wide and extends far downstream from the actuator. At this actuator amplitude, the

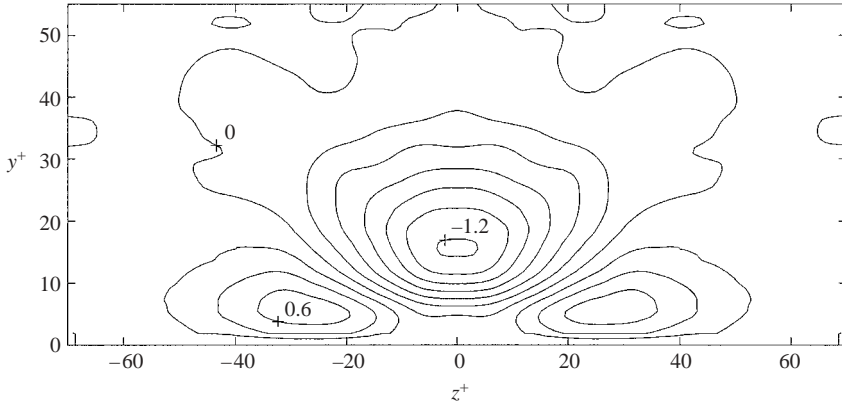


FIGURE 9. Contour plot of the local change in the mean streamwise velocity resulting from fixed-amplitude forcing of the flow by the actuator. $x = 60l^*$ downstream of the end of the actuator slit which is at $z^+ = 0$.

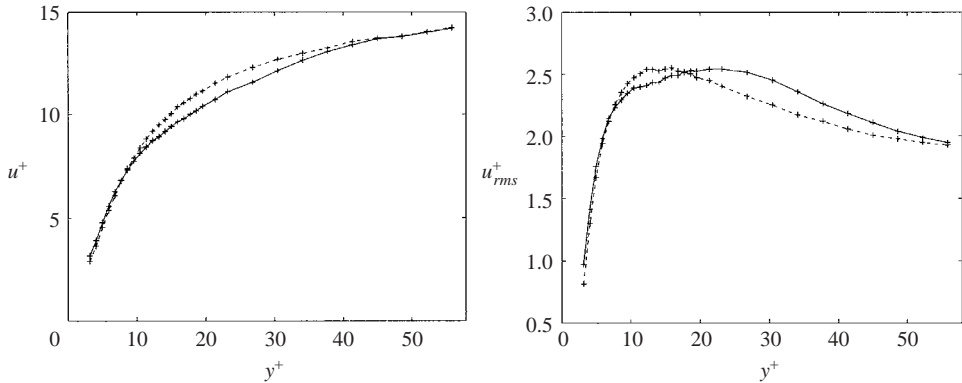


FIGURE 10. Mean and r.m.s. streamwise velocity profiles, $60l^*$ downstream of the actuator. The injection of low-speed fluid is seen in the mean profile, while the r.m.s. profile shows a maximum value located further away from the wall in the forced case (solid line: forced, dashed line: unforced).

maximum velocity defect is approximately $1.2u_\tau$. On either side, a region of high-speed fluid is observed where the downward motion of the vortex pair drags high-streamwise-momentum fluid towards the wall. Further details of the characteristics and evolution of these vortices were measured and are discussed by Lorkowski *et al.* (1997).

The mean and root-mean-squared streamwise velocity profiles downstream of the actuator are shown in figure 10. Figure 10(a) is a plot of the mean profile taken downstream of the actuator and along the centreline. It illustrates the region of lower-speed fluid that results from the actuator jet. The root-mean-squared profile (figure 10b) shows that the maximum fluctuation intensity remains roughly constant, but is shifted away from the wall.

3.4. Active control

Rathnasingham & Breuer (1997b) presented results on the effect of steady (fixed-amplitude) forcing on the control signal (the r.m.s. streamwise velocity fluctuation), and found that there was an optimum actuation amplitude of $1.3u_\tau$ where the u'_{rms}

amplitude was reduced by 10%. However, they also found that the same configuration (three sensors, one actuator) operating in a real-time feedforward mode reduced the u_{rms} by 34% (at approximately the same average actuation amplitude). It is this improvement that we seek to explore in more detail in the next section.

In the present experiments, two control objectives were examined. The bulk of the experiments were aimed at minimizing the streamwise velocity fluctuations at a point, or points, in the near-wall region (at $y^+ = 12$). Although this is not a very practical objective for eventual applications, it was convenient for these demonstration experiments since the control signal was obtained from a hot-wire probe which could be easily moved throughout the boundary layer. A second series of control experiments were also conducted. These were aimed at minimizing the r.m.s. wall-pressure signal, with the goal of lowering turbulence-induced wall pressure fluctuations. This has more direct application, but is harder experimentally, since wall pressure signals are only available at discrete points and moving the wall pressure transducer is not experimentally convenient.

The multiple-input/multiple-output (MIMO) prediction procedure described earlier was used together with the pre-conditioning of all three detection sensors to emphasize the large-scale motion (as in figure 5*d*). Control was applied using both a single actuator (as was demonstrated by Rathnasingham & Breuer 1997*b*) as well as three actuators together. In order to assess the differences between the single and multiple actuator systems, the control was enforced at a single control point, located immediately downstream of the centre actuator. Finally, the three-sensor, three-actuator system was used to control the flow at three control points, each located behind an actuator.

3.4.1. Implementation details

The FIR filters described above were initially derived using as many as 128 coefficients. However, the simple structure of the filter shown in figure 7 suggests that we do not need to retain so many coefficients. Indeed, from a practical perspective, it is desirable to use a lower number of coefficients so that the control system can be efficiently implemented in the digital signal processing hardware. Standard techniques for filter-order reduction were used to reduce the number of coefficients required while still maintaining filter accuracy. A polynomial was used to approximate the spectral performance of the full filter and this was then transformed back to a low-order FIR representation suitable for DSP implementation. It was found that the full filter (which was derived using either 64 or 128 coefficients) could be accurately represented using an FIR filter of order 32. This low-order representation exhibited an r.m.s. error (in frequency space) of less than 5% when compared to the full-order filter. Even lower-order filters could be achieved using IIR techniques, but for simplicity, and in order to ensure a linear phase response, FIR filters were used and had more than adequate performance in the current experiment.

3.5. Effect of control on mean flow characteristics

Figures 11 and 12 show the streamwise and wall-normal extent of the controlled flow downstream and above the actuator array. In both cases three sensors are used and the performance of a single actuator MISO system is compared with the performance of the full three-actuator MIMO system. It can be seen that the control performance is maximized at the control point, with approximately 25% reduction in the r.m.s. fluctuations, and that the reductions in the r.m.s. u -fluctuations degrade slowly as one moves both downstream and away from the wall.

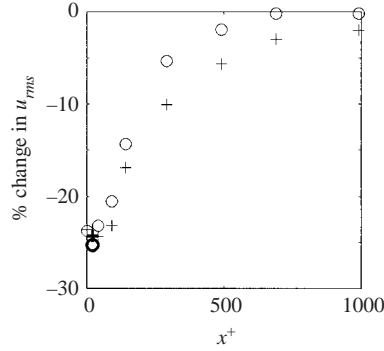


FIGURE 11. Percentage change in the streamwise velocity fluctuation as a function of the streamwise distance from the centre actuator. The circles represent the control achieved using a single actuator while the pluses represents the control achieved using three actuators. The control is weighted to favour a single control point, $300l^*$ downstream from the centre of the actuator array. The bold circle and plus indicate the points of optimization ($x^+ = 20$).

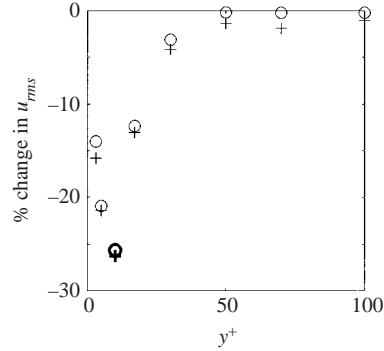


FIGURE 12. Percentage change in the streamwise velocity fluctuations as a function of the distance away from the wall and above the control point. The circles represent the control achieved using a single actuator while the pluses represents the control achieved using three actuators. The control is weighted to favour a single control point, $300l^*$ downstream of the centre of the actuator array. The bold circle and plus indicate the points of optimization ($y^+ = 15$).

Although the additional actuators result in only a marginal improvement in the control performance at the control point (about 4%), the MIMO system improves the overall system performance in the sense that the range of controlled flow is extended over the actuator footprint. In addition, at any given x -location downstream of the control points, the local reduction in u_{rms} is improved (figure 11). However, the addition of multiple actuators is not ‘felt’ in the wall-normal direction (figure 12) suggesting that the control is effective only in the near-wall region ($y^+ < 50$). This is expected, since the disturbances created by the actuators do not penetrate beyond this near-wall region and, moreover, the majority of the coherent structures that the actuators are presumably acting on are known to be located within this near-wall region.

The effect of multiple actuators on the spanwise distribution is more pronounced (figure 13). Here, the measurements are taken in a spanwise plane level with the control point ($x^+ = 20$ downstream of the actuator array). The reductions in u -fluctuations

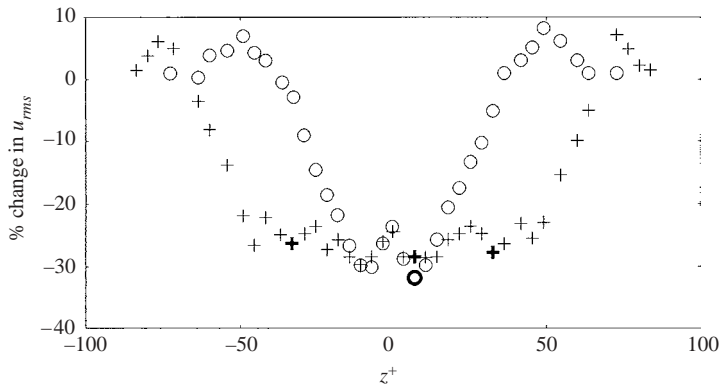


FIGURE 13. Percentage change in the streamwise velocity fluctuations due to control. The probe is traversed at $y^+ = 12$ in the spanwise direction just downstream ($x^+ = 20$) of the control point location. The circles represent the control achieved using a single actuator while the pluses represent the control achieved using three actuators. The bold pluses and circle indicate the points of optimization ($z^+ = 5$ and $z^+ = 45$).

degrade gradually, over approximately $50l^*$, and there is a small overshoot at the edge of the controlled region where the fluctuations are about 5% greater than the uncontrolled flow. When three actuators are employed, the controlled region is extended to cover the entire plane behind the actuator array, and the relaxation to the uncontrolled flow is shifted out accordingly. It is encouraging that the spanwise spacing of the actuators ($40l^*$) seems about right in that the fluctuations are uniformly reduced over the span of the actuator array, but appear to be rising slightly at $z^+ = 40$ – just at the point where the next actuator is located. As in the streamwise profile, the maximum reduction remains unchanged from the single-actuator case, but the added control provided by the adjacent actuators extends the spanwise control area. This indicates that additional actuators placed in the array may be used to expand the control region further in the spanwise direction. The appropriate spanwise separation may be estimated from the extent of the single-point control and is approximately $40l^*$.

Figure 14 shows the spanwise structure behind the actuator plane. A gentle relaxation is observed in which the centreline re-adjusts somewhat slower than the edges which quickly move back to their uncontrolled state due to entrainment of uncontrolled turbulent flow at the edge of the controlled region. By mapping this relaxation to the uncontrolled state, we find that the controlled zone shrinks with a converging angle of approximately 6° .

Figure 15 illustrates this converging pattern in relation to the actuators and control points (drawn to scale). This zone of influence of this particular configuration may be used to determine the appropriate spacing between actuators and control points for broadening the region of control.

3.5.1. Effects on the mean wall shear stress

There is ample evidence (for example, Johansson & Alfredsson 1982) to suggest that there exists a strong relationship between the so-called coherent structures and the local wall shear stress. In addition there is considerable interest in using active control to reduce the mean wall shear stress (the drag due to the turbulent boundary layer). For these reasons, it was of interest to investigate the effect of the control on the wall shear stress (i.e. drag). This effect was assessed by estimating the slope of the

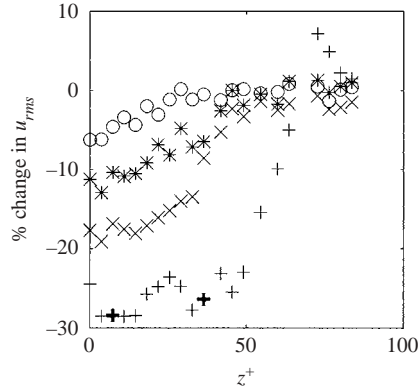


FIGURE 14. Percentage change in the streamwise velocity fluctuation with spanwise distance from the centre actuator at four streamwise stations downstream of the actuator array; $x^+ = 20$ (+), 100 (\times), 300 ($*$) and 500 (\circ). The bold pluses indicate the points of optimization ($z^+ = 5$, $z^+ = 45$).

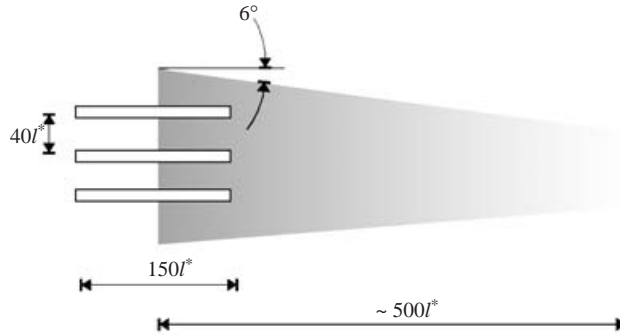


FIGURE 15. Schematic illustration of the zone of controlled flow downstream of the three actuators.

mean velocity profile near the wall. Figure 16(a) is a plot of the mean velocity profile for the unforced and forced cases taken at $z^+ = 10$. By interpolation of the profile, we find a reduction in the estimated wall shear stress of approximately 7%. We should stress that the control objective in the current experiments was not changed, but remained the minimization of the r.m.s. u -fluctuations at $y^+ = 12$. In addition, the measurement of the velocity profile is only a crude estimation of the wall shear. Nevertheless, in this case the measurement was taken with the hot wire fixed at each y -location while the control system was switched from off to on and off again, and so the uniform reduction in mean velocity does suggest that mean drag reduction is achieved. Figure 16(b) shows the change in the mean streamwise velocity in the spanwise direction, taken at $y^+ = 15$ (set with the control system off). It shows a marked and uniform reduction over the control region, again supporting the idea that the mean shear is reduced over the entire control region. However, we stress that this needs to be investigated further.

3.6. Control of wall pressure signal

As mentioned earlier, a parallel series of experiments aimed at the control of the wall pressure fluctuation were carried out in a similar fashion to that of the

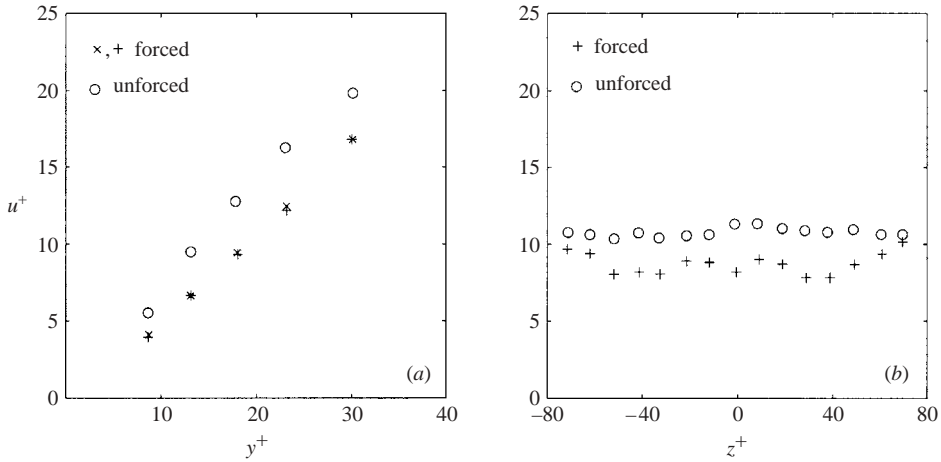


FIGURE 16. Mean velocity, measured near the wall, for the forced and unforced cases: (a) in the wall-normal direction at $z^+ = 10$; the estimated wall shear stress is reduced by approximately 7% in the forced case; (b) in the spanwise direction, at $y^+ \approx 15$, the velocity in the controlled flow is reduced throughout the control region.

streamwise velocity fluctuation control described thus far. The wall pressure at the downstream control points was characterized using the upstream shear sensors and control was achieved with three configurations: single-input/single-output (SISO), multiple-input/single-output (MISO) and multiple-input/multiple-output (MIMO). The results of these experiments are briefly mentioned here, primarily to indicate the generality of the control methodology. In all cases, the control objective was to minimize the r.m.s. pressure fluctuations.

A SISO configuration, as illustrated in figure 5(a) was first investigated. In this case, the conditioned pressure signal, $500l^*$ downstream of the detection sensors, was used as the control variable and a reduction of 17% in p_{rms} was obtained. With this result, a MISO configuration (figure 5d) was implemented, in which case the additional information obtained from the adjacent sensors improved the controllability of the flow (as in the case with the streamwise velocity fluctuations), and p_{rms} at the control point was reduced by 20%. Finally, a MIMO control scheme was implemented in which the r.m.s. signals at three pressure sensors, $500l^*$ downstream of the detection sensors, were minimized using three shear sensors and three actuators. The performance of the controller in reducing the pressure fluctuations was similar to that for the streamwise velocity, in that the maximum reduction was less than in the single-output case but the control affected a larger area. The reduction in p_{rms} was 15% at the middle sensor and 12% at the adjacent ones, $40l^*$ in the spanwise direction. Scans of the pressure signal at other locations in the boundary layer were not attempted in this study.

3.7. Effects of active control on turbulence structure

While the success of real-time control on the mean flow has clearly been demonstrated in the previous section, it is of interest to understand how the structure of the turbulent flow has been modified by the introduction of the control system. In order to address this, common measures of the boundary layer turbulent structure were taken: the spanwise correlation of streamwise velocity as well as conditional averages

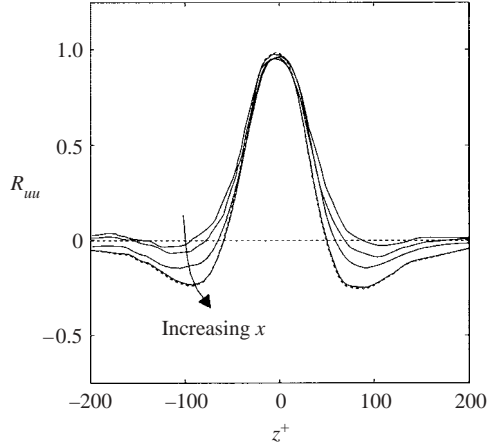


FIGURE 17. Spanwise spatial correlation of the streamwise fluctuation velocity, R_{uu} , measured at several stations downstream of the actuator array.

of streamwise velocity and the bursting frequency, as determined from variable interval time average (VITA) techniques (Blackwelder & Kaplan 1976).

The spanwise spatial correlation at four streamwise stations downstream of the actuator array is shown in figure 17. The correlation corresponding to the unforced flow is shown by the dashed line. At the point of optimization ($x^+ = 20$), the location of the minimum point and the point of zero crossing have been forced out further in the spanwise direction. This indicates that the large-scale structures that now exist, after the application of the control system are more widely spaced in the spanwise direction. They are also more weakly correlated, as indicated by reduced amplitude of the minimum point in R_{uu} . The correlation curve recovers to the unforced curve as the streamwise station moves further downstream, and the effect of the control wears off. The implication of this modification of the spatial correlation is that the effect of the control system is to weaken the intensity of the streaks and to increase (or perhaps randomize) the spanwise spacing of the near-wall streaks. These actions interrupt the natural turbulence production mechanisms, reducing the turbulence intensity.

3.7.1. Effects on inclined shear layer frequency

Another measure of the effect of the active control on the structures in the turbulent boundary layer is changes in the frequency of high-amplitude streamwise accelerations, also known (for historical reasons) as the ‘bursting frequency’. With the benefit of numerical simulations of turbulent wall-bounded flows, it is clear (e.g. Johansson *et al.* 1991) that the ‘bursting’ events detected using the VITA technique (Blackwelder & Kaplan 1976) are generally not related to any physical bursting process, but rather are associated with sharp accelerations in the streamwise velocity which in turn are a signature of inclined shear layers correlated with local turbulence production (Johansson *et al.* 1991). While direct numerical simulations have the ability to closely examine changes in the entire flow field, experiments must rely on data from a single or at best a few spatial locations, and thus measured changes in the bursting frequency are (in the absence of true Reynolds stress measurements) a reasonable indication of the strength and frequency of flow structures associated with turbulence production in the boundary layer.

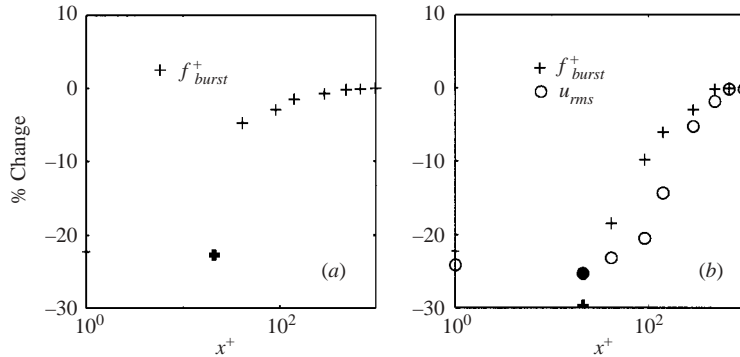


FIGURE 18. Percentage reduction in bursting frequency with streamwise distance from the centre of the actuator (*a*) using a threshold level of 3 times the local u_{rms} and (*b*) a threshold level of 3 times the unforced u_{rms} . The control point is marked in bold.

In the present case, the bursting frequency was computed from a long time series, using the VITA technique (Blackwelder & Kaplan 1976). Following the recommendations of Alfredsson & Johansson (1984), the averaging time was chosen to be $20t^*$ which was comparable to the outer time scale (computed using the free-stream velocity and the local displacement thickness of the boundary layer) of $18.5t^*$.

The conditional averages of the wall pressure and velocity events in the uncontrolled flow were measured and were seen to agree well with previous results of Alfredsson & Johansson (1984). In addition, the variation of the bursting frequency f^+ with the threshold parameter k also agrees well with previous results of Blackwelder & Haritonidis (1982) and Alfredsson & Johansson (1984).

With this validation complete, a comparison was made between the bursting frequency in the controlled and uncontrolled boundary layer to evaluate the effect of control on the large-scale shear layer structures. At the control point (at the downstream end of the actuator), the bursting frequency was observed to decrease by approximately 23% for all threshold parameters, k , greater than about 2. This suggests that the control was effective in breaking up the more intense shear layer structures, but had a less pronounced effect on the weaker accelerations that are associated with smaller or less well-developed structures. However, this reduction was found to be localized and the flow is seen to return to close to the unforced case quite rapidly. This recovery to the unforced case is illustrated in figure 18(*a*) which shows the reduction in burst frequency, calculated with a threshold level of 3, versus downstream distance. One clearly sees how the bursting frequency starts to recover very quickly following the control point and then, more slowly, returns to its unforced level. This result is somewhat puzzling given the observation (figure 11) that the reduction in u_{rms} persists much further downstream. To explore this further, the bursting frequency is computed with a threshold level that is based on the baseline (unforced) u_{rms} , rather than the local u_{rms} as in the previous case. This provides an indication of how the bursting frequency of events of a fixed amplitude (i.e. 3 times the unforced u_{rms}) are affected by the control. Figure 18(*b*) shows the reduction of the bursting frequency with x^+ , computed with the unforced threshold level, plotted (using pluses) together with the reduction in u_{rms} (indicated with circles). The data show that there is a similar evolution in x of both quantities, indicating that they may be in some sort of local equilibrium. Thus, we conjecture that at the control point (marked in bold), the flow undergoes an aggressive modification, resulting in a

sharp decrease in the strength and frequency of turbulence-producing structures (as measured by the observed reduction in the bursting frequency). As this modified flow advects downstream, both the structures and the overall level of turbulence recover together, reaching their unforced levels several $100l^*$ downstream.

4. Concluding remarks

The formulation and implementation of an active control algorithm for a turbulent boundary layer has been presented with encouraging results. The control scheme is based on an active matrix of sensors and actuators that are networked through linear filters that optimally predict the evolution of large-scale structures in the near-wall region. Similar filters that model the characteristics of the actuators and their effect on the flow are also used, and the combination of the forward prediction and actuation is used to minimize a cost function defined from the signal measured at a series of control points further downstream. In the present case, two control objectives were pursued: first, the linear cancellation of streamwise velocity fluctuations at a series of control points in the buffer layer and secondly the minimization of wall pressure fluctuations at a single point downstream of the actuator array.

The effect of the active control is to disrupt the turbulence-generating cycle, as outlined for example by Johansson *et al.* (1991), Adrian, Meinhart & Tomkins (2000) or Schoppa & Hussain (2002). This cycle is dominated by the formation, intensification and decay of elongated streaks (or hairpin vortices), and it seems reasonable to assume that the success of the active control scheme is due to its ability to identify these naturally occurring structures as they advect in the near-wall region, and to modify them, by weakening them (as evidenced by the change in the spanwise correlation), perhaps by disrupting their natural evolutionary cycle (as evidenced by the reduction in bursting frequency). The actuators in the present study were specifically designed to introduce a 'synthetic' streak which acts to counteract the near-wall structures. However, without significantly more detailed measurements or simulations it is currently impossible to determine exactly how the boundary layer structure has been changed or how the control can be improved. Follow-on experiments are currently underway, and initial computations that simulate the realistic shape and performance of actuators have been reported by Lee & Goldstein (2001).

The formal control system has a number of attractive features. It is quite general, and can be applied to a wide variety of flow control problems, both local and distributed. The sensor inputs can be chosen from both temporal and spatial templates. In the case of a purely temporal template, the predictive filters are simply the two-point correlations between the sensors and the control points. The system can be implemented using available DSP or computer hardware, and in future implementations the filters could even be implemented using analog components – making widespread deployment a realistic possibility.

The limitations of the scheme stem from the idealized assumption of linearity made both in the system identification and the control. Other non-ideal behaviour in the system comes from the lack of information about the flow field, due to the practical limitations placed on the number of sensors and their capabilities. The sensors used here are sensitive to spanwise shear fluctuations but due to the rectification of the hot wire do not differentiate between positive and negative fluctuations. The actuators are also limited to only positive ejections into the boundary layer (except at low amplitude when they become reversible). This rectification of the sensors and actuators inhibited

realization of the full potential of the control scheme. Nevertheless, the control results were far better than expected in terms of the suppression of the turbulence fluctuations and the spatial extent of the controlled flow. The streamwise velocity fluctuations were reduced by up to 30% and extended for several hundred viscous lengths in the streamwise direction and approximately 150 and 50 viscous lengths in the spanwise and wall-normal directions respectively. By comparing the reduction in the streamwise turbulent fluctuation energy (measured over a z, y -plane above the control points) to the kinetic energy introduced by the actuators, we can crudely estimate the control efficiency, which was found to be 50:1. This result is intended as an order-of-magnitude estimate only, and does not include the electrical power required to drive the sensors, actuators or signal processing.

The wall pressure fluctuations and the mean wall shear stress (drag) were also reduced by up to 15% and 7% respectively. In the latter case, this was not the control objective, but was realized as a by-product. We suspect that if wall-shear reduction were implemented as the primary control objective, even better performance will be achieved. It is important to acknowledge that, even though control is enforced at a discrete number of control points, the benefits of control extend over a wide spatial area. This is not the case in some other active control problems, most notably the active control of sound, in which a quiet zone is often achieved over a small area but at the expense of significant noise enhancement away from the control area. The current scheme does not suffer from this problem, primarily due to the fact that the control is not based on localized phase cancellation as is the case of anti-noise techniques.

Due to the strongly convective nature of the turbulent boundary layer, and the negligible acoustic feedback, the actuators do not affect the signals measured by the upstream sensors, and consequently a feedforward algorithm can be employed (as defined by Nelson & Elliot 1992). Such active control is an important step up in both complexity and performance from fixed-amplitude (sometimes called open-loop) actuation. Such control architectures are also well-suited for adaptive feedback in which the error from the downstream control points can be used to improve the overall control performance in some iterative manner. In the present case, only a crude manual adaptation of the filter gain and phase was tested, and found to be unnecessary. We believe that this only reflects the stable testing environment in which the experiments were conducted. In a 'real' configuration, small changes in wind speed, temperature, pressure gradient, etc. will inevitably take place and adaptation will be essential. Several techniques already exist for this, based on local optimization of the cost function with respect to the filter weights. These will be implemented and tested in the next series of experiments.

From a scientific standpoint, the most interesting aspect of this work is the surprisingly successful performance of a linear controller in the chaotic, nonlinear turbulent boundary layer. This idea – that the structures in a turbulent boundary layer respond to the mean shear in a linear manner – has been proposed many times and in different guises, most notably by Landahl (1990). However, these results, along with other recent results from numerical control experiments (Lee *et al.* 1997) add weight to this view. Future improvements to this scheme must include the addition of a better forward prediction, using the dynamics of the near-wall flow (i.e. a Kalman filter based on the Navier–Stokes or the linearized equations of motion) and the expansion of the control matrix to give a larger region of controlled flow. Another critical question is that of Reynolds number scaling. It has been implicitly assumed that the layout of the sensors and actuators and the bandwidth of the control system

all scale with wall variables. Such Reynolds number scaling studies are very hard to conduct in a physical experiment because as the Reynolds number changes, so does the non-dimensional size of any fixed system of sensor and actuator hardware. Nevertheless, these issues are of critical importance and should be investigated in future studies.

This work was supported by the Office of Naval Research, grant N00014-92-J-1918 monitored by Dr L. Patrick Purtell. The authors would also like to acknowledge Thomas Lorkowski for his help in measuring the fixed-amplitude actuator performance. Stuart Jacobson and Jim Paduano provided many valuable suggestions during the course of the work. We would also like to pay particular tribute to the memory of Mårten Landahl who long advocated the concept that linear processes are important in the turbulent boundary layer, and whose insight and vision helped to shape many of the ideas that are reflected in this paper.

REFERENCES

- ADRIAN, R. 1994 Stochastic estimation of conditional structure – A review. *Appl. Sci. Res.* **54**, 291–303.
- ADRIAN, R., MEINHART, C. & TOMKINS, C. 2000 Vortex organization in the outer region of the turbulent boundary layer. *J. Fluid Mech.* **422**, 1–54.
- ALFREDSSON, P. H. & JOHANSSON, A. V. 1984 On the detection of turbulence-generating events. *J. Fluid Mech.* **139**, 325–345.
- ALMONLIRDVIRMAN, K. A. & BREUER, K. S. 2000 Linear predictive filtering in a turbulent channel flow. *Phys. Fluids* **12**, 3221–3229.
- BENDAT, J. & PERSOL, A. 1971 *Random Data: Analysis and Measurement Procedures*. Wiley-Interscience.
- BEWLEY, T., MOIN, P. & TEMAM, R. 2001 DNS-based predictive control of turbulence: an optimal benchmark for feedback algorithms. *J. Fluid Mech.* **447**, 179–225.
- BLACKWELDER, R. F. & HARITONIDIS, J. H. 1982 The bursting frequency in turbulent boundary layers. *J. Fluid Mech.* **132**, 87–103.
- BLACKWELDER, R. F. & KAPLAN, R. E. 1976 On the wall structure of the turbulent boundary layer. *J. Fluid Mech.* **76**, 89–112.
- BREUER, K., DZENITIS, M., GUNNARSSON, J. & ULLMAR, M. 1996 Linear and nonlinear evolution of roughness-induced disturbances in a laminar boundary layer. *Phys. Fluids* **8**, 1415–1423.
- BROWN, R. G. & HWANG, P. Y. C. 1997 *Introduction to Random Signals and Applied Kalman Filtering*. John Wiley & Sons.
- CHOI, H., MOIN, P. & KIM, J. 1994 Active turbulence control for drag reduction in wall-bounded flows. *J. Fluid Mech.* **262**, 75–110.
- COLLER, B. D., HOLMES, P. & LUMLEY, J. L. 1994 Control of bursting in boundary layer modes. *Appl. Mech. Rev.* **47** (6, Part 2), 139–149.
- GAD-EL-HAK, M. & BLACKWELDER, R. F. 1989 Selective suction for controlling bursting events in a boundary layer. *AIAA J.* **27**, 308–314.
- GLEZER, A. & AMITAY, M. 2002 Synthetic jets. *Annu. Rev. Fluid Mech.* **34**, 503–529.
- HUNT, J. & CARRUTHERS, J. 1990 Rapid distortion theory and the problems of turbulence. *J. Fluid Mech.* **212**, 497–532.
- INGARD, U. 1953 On the theory and design of acoustic resonators. *J. Acoust. Soc. Am.* **25**, 1037–1060.
- JACOBSON, S. A. & REYNOLDS, W. C. 1998 Active control of streamwise vortices and streaks in boundary layers. *J. Fluid Mech.* **360**, 179–211.
- JOHANSSON, A. V. & ALFREDSSON, P. H. 1982 On the structure of turbulent channel flow. *J. Fluid Mech.* **122**, 295–314.
- JOHANSSON, A. V., ALFREDSSON, P. H. & KIM, J. 1991 Evolution and dynamics of shear layer structure in near wall turbulence. *J. Fluid Mech.* **224**, 579–599.
- JOHANSSON, A. V., HER, J. & HARITONIDIS, J. H. 1987 On the generation of high amplitude wall-pressure peaks in turbulent boundary layers and spots. *J. Fluid Mech.* **175**, 119–142.

- KRAVCHENKO, A. G., CHOI, H. & MOIN, P. 1993 On the relationship between near-wall streamwise vortices to wall skin friction in turbulent boundary layers. *Phys. Fluids* **5**, 3307–3309.
- LANDAHL, M. T. 1990 On sublayer streaks. *J. Fluid Mech.* **212**, 593–614.
- LEE, C. & GOLDSTEIN, D. 2001 DNS of microjets for turbulent boundary layer control. *AIAA Paper* 2001-1013.
- LEE, C. & GOLDSTEIN, D. 2002 Two-dimensional synthetic jet simulation. *AIAA J.* **40**, 510–516.
- LEE, C., KIM, J., BABCOCK, D. & GOODMAN, R. 1997 Application of neural networks to turbulence control for drag reduction. *Phys. Fluids* **9**, 1740–1747.
- LORKOWSKI, T., RATHNASINGHAM, R. & BREUER, K. S. 1997 Small-scale forcing of a turbulent boundary layer. *AIAA Paper* 97-1792.
- NAGUIB, H., GRAVANTE, S. & WARK, C. 1996 Extraction of turbulent wall-pressure time-series using an optimal filtering scheme. *Exps. Fluids* **22**.
- NELSON, P. & ELLIOT, S. 1992 *Active Control of Sound*. Academic.
- PODVIN, B. & LUMLEY, J. 1998 Reconstructing the flow in the wall region from wall sensors. *Phys. Fluids* **10**, 1182–1190.
- PURTELL, L., KLEBANOFF, P. & BUCKLEY, F. 1981 Turbulent boundary layers at low Reynolds numbers. *Phys. Fluids* **24**, 802–811.
- RATHNASINGHAM, R. 1997 System identification and active control of a turbulent boundary layer. PhD Thesis, Department of Aeronautics and Astronautics, MIT (Also *MIT FDRL Rep.* 97-6).
- RATHNASINGHAM, R. & BREUER, K. S. 1997a Coupled fluid-structural characteristics of actuators for flow control. *AIAA J.* **35**, 832–837.
- RATHNASINGHAM, R. & BREUER, K. S. 1997b System identification and control of turbulent flows. *Phys. Fluids* **9**, 1867–1869.
- SCHWEWE, G. 1983 On the structure and resolution of wall-pressure fluctuations associated with turbulent boundary layer flow. *J. Fluid Mech.* **134**, 311–328.
- SCHLICHTING, H. 1968 *Boundary Layer Theory*. McGraw-Hill.
- SCHOPPA, W. & HUSSAIN, F. 1998 A large-scale control strategy for drag reduction in turbulent boundary layers. *Phys. Fluids* **10**, 1049–1051.
- SCHOPPA, W. & HUSSAIN, F. 2002 Coherent structure generation in near wall turbulence. *J. Fluid Mech.* **453**, 57–108.
- TSAO, T., JIANG, F., MILLER, R., TAI, Y., GUPTA, B., GOODMAN, R., TUNG, S. & HO, C. 1997 An integrated mems system for turbulent boundary layer control. In *Technical Digest, 1997 Intl Conf. on Solid-State Sensors and Actuators (Transducers '97)*, Chicago, IL, vol. 1, pp. 315–318.
- WALEFFE, F. 1997 On a self-sustaining process in shear flows. *Phys. Fluids* **9**, 883–900.
- WILKINSON, S. & BALASUBRAMANIAN, R. 1985 Turbulent burst control through phase-locked traveling surface depression. *AIAA Paper* 85-0536.
- WU, K. & BREUER, K. 2003 Dynamics of synthetic jet arrays for closed-loop flow control. *AIAA Paper* 2003-4257.